Electron and phonon confinement and surface phonon modes in CdSe–CdS core–shell nanocrystals

2005 J. Phys.: Condens. Matter 17 5697

(http://iopscience.iop.org/0953-8984/17/37/008)

INSTITUTE OF PHYSICS PUBLISHING JOURNAL OF PHYSICS: CONDENSED MATTER

J. Phys.: Condens. Matter **17** (2005) 5697–5708 doi:10.1088/0953-8984/17/37/008

Electron and phonon confinement and surface phonon modes in CdSe–CdS core–shell nanocrystals

A Singha[1], **B Satpati**[2], **P V Satyam**[2] **and Anushree Roy**[1]

[1] Department of Physics, Indian Institute of Technology, Kharagpur 721 302, WB, India
[2] Institute of Physics, Bhubaneswar 751005, India

E-mail: anushree@phy.iitkgp.ernet.in

Received 12 July 2005, in final form 8 August 2005
Published 2 September 2005
Online at stacks.iop.org/JPhysCM/17/5697

Abstract

The optical and vibrational properties of bare and CdS shelled CdSe nanocrystalline particles are investigated. To confirm the formation of such nanocrystals in our samples we estimate their average particle sizes and size distributions using TEM measurements. From the line profile analysis of the HRTEM images the core–shell structure in the particles has been confirmed. The blue shift in the optical absorption spectra, analysed using theoretical estimates based on the effective bond order model, establishes the electron confinement in the nanoparticles. The main aim of this paper is to show the unique characteristics of the nanocrystals (which are absent in the corresponding bulk material), such as confinement of optical phonons and the appearance of surface phonons. Making use of the dielectric continuum model we are able to match the experimental and theoretical values of the frequencies of the surface phonons. We believe that our studies using optical probes provide further evidence for the existence of core–shell structures in CdSe–CdS type materials.

1. Introduction

Over the last couple of decades, unique physical properties due to quantum confinement effects have been reported for a wide range of semiconductor nanocrystalline materials [1]. Since in these systems the surface to volume ratio is high compared to that of corresponding bulk materials, surface states play a crucial role in determining their physical properties. The surface of nanocrystals is made of atoms that are not fully coordinated. Hence, they are highly active, and these surface atoms act like defect states unless they are passivated by either organic ligands or higher bandgap semiconductor materials [1, 2]. Thus, the current direction in this field of research includes modification of given size-quantized semiconductor particles by means of surface chemistry. Coating nanoparticles by another material yields core–shell

nanocrystals [1]. In the literature, we find discussion on core–shell nanocrystalline structures due to surface modifications of the particles.

In a core–shell structure, like inorganic epitaxial shell growth, the organic ligands cannot passivate both cationic and anionic surface sites of the core [3]. The particles passivated by inorganic shell structures are more robust than organically passivated nanocrystals and have greater tolerance to the processing conditions necessary for incorporation into solid structures [4]. For effective surface passivation, the core particles having a certain bandgap are capped with a higher bandgap material. Moreover, the conduction band energy of the capping (shell) material is usually higher than that of the core material, with the valence band energy of the capping material being lower. This energetic situation is called a type-I structure [1]. Due to the presence of higher bandgap capping material, the photogenerated excitons in the core remain localized in the same region and are forced to recombine while spatially confined in the core. Confinement of electrons in the nanocrystals gives rise to a blue shift in the optical absorption and PL spectra of the material. As the non-radiative decay channels through surface states are not accessible for these electrons, core–shell structures thus formed show higher luminescence quantum yield [2, 3, 5–10], lower fluorescence lifetime [9], and many other benefits [11] related to the tuning of the bandgap in two materials.

Like electrons, phonons are also confined in nanocrystals. In bulk crystals, the phonon eigenstate is a plane wave, and the wavevector selection rule for the first-order Raman scattering requires $q \sim 0$. In contrast, the spatial correlation function of the phonon becomes finite due to its confinement in the nanocrystal and hence the $q \sim 0$ selection rule gets relaxed. In general, the phonon-dispersion curves of bulk crystals show the frequency ω to be a decreasing function of wavevector q. Hence, the first-order Raman line shifts and broadens towards the low-frequency side for the nanocrystals. This has been proposed and explained by a phonon confinement model [12]. Confinement of phonons for Si, Ge, BN, CdS, CdS_xSe_{1-x} and many other nanocrystals has been reported in the literature [13–18].

As mentioned before, surface states play an important role in deciding the different physical properties of nanocrystals. For a plane wave propagating in the x-direction in a bulk crystal, the temporal and spatial variation of the wave is described by the factor $\exp[\mathrm{i}(kx - \omega t)]$, where the wavevector $k = (\omega/c)\sqrt{\epsilon(\omega)}$; $\epsilon(\omega)$ is the dielectric constant of the crystal. In the frequency range between bulk longitudinal optical (LO) phonon frequency, ω_{LO}, and transverse optical (TO) mode frequency, ω_{TO}, $\epsilon(\omega) < 0$, k is imaginary. Therefore, in this frequency range the wave decays exponentially in the medium, i.e. it cannot propagate in bulk crystals and only surface modes exist [19]. Because of the enhanced surface to volume ratio these modes appear for nanocrystals, and they provide relevant information on the surface states. Recently, the surface phonon modes in ZnS shelled CdSe particles have been reported [20].

The characteristics of bare CdSe nanocrystals are now well established. CdSe nanocrystals passivated with a long organic chain (like TOPO) have room-temperature photoluminescence (PL) (quantum yield 10%) with a very long fluorescence time [21, 22]. The inorganic shelling of the CdSe core by CdS has also been explored and shown to be better for surface passivation [3, 23–25]. Previous high-resolution transmission electron microscopy (HRTEM) and x-ray photoelectron spectroscopy measurements have shown that shell growth in this system does not form an alloy [3, 26]. The lattice mismatch of 3.9% between CdS and CdSe is small enough to allow epitaxial growth while still preventing alloying. Moreover, the difference in bandgap (2.42 eV for CdS and 1.74 eV for CdSe at room temperature) is large enough for shell growth. The room-temperature PL yield for the CdSe–CdS core–shell system has been reported to be up to 50% [3]. The electronic structure in this material can be understood from a molecular orbital model and a particle in a box model, as discussed in [3]. The same electronic structure has also been discussed from the analysis of photoelectron spectra from

the core–shell structure [26]. The high photostability of the system has been explained by confinement of electrons and holes in the core–shell region.

In this paper, we discuss the optical properties of marcaptoacetic acid stabilized bare CdSe particles and CdS capped CdSe particles. The nanoparticles have been characterized by their absorption spectra as well as by HRTEM images. The optical transition is modelled using an effective bond order model (EBOM). The average particle size and size distribution of the particles have been estimated from both transmission electron microscopy (TEM) images and optical absorption measurements; these have been further supported by Raman measurements. We have quantitatively analysed asymmetric Raman line shapes including both confined optic modes and surface phonon modes. The observed frequencies of the SP modes in these systems have been compared with the calculations based on the dielectric continuum model. In section 2 of this paper, we briefly discuss the sample preparation procedure which we have followed. Section 3 deals with analysis of TEM/HRTEM images of the samples. Section 4 demonstrates the optical properties of the samples, studied by optical absorption spectroscopy. Detailed analysis of the phonon spectra is reported in section 5. Finally, in section 6, we have summarized our results with a few concluding remarks.

2. Sample preparation

We followed a well-established chemical route to prepare the nanoparticles [27].

2.1. Chemicals

For sample preparation, we used highly pure reagents cadmium perchlorate, marcaptoacetic acid, sodium sulfide, anhydrous sodium sulfite, solid selenium powder and sodium hydroxide.

2.2. Preparation of stock solution of Na_2SeSO_3

1.0 g of Se powder was added to 200 ml (1.1 M) hot Na_2SO_3 solution under stirring conditions and then boiled for half an hour. Subsequently, the solution was cooled at room temperature and the aqueous layer was filtered using Whatman filter paper. This solution is used as the stock solution.

$$Na_2SO_3 + Se \rightarrow Na_2SeSO_3.$$

2.3. Preparation of marcaptoacetic acid stabilized CdSe nanocrystals: sample A

Following Liu *et al* [27], 150 ml of $Cd(ClO_4)_2$ (2×10^{-4} M) and 150 ml of HS–CH_2–COOH (2×10^{-4} M) were mixed and stirred vigorously for about 5 min. Here, the latter acts as a stabilizing agent. The pH of the solution was adjusted to 9.0 by adding aqueous NaOH (1.0 M) solution and heated to 100 °C under N_2 atmosphere. Subsequently, 0.5 ml of Na_2SeSO_3 was added dropwise to the solution which was boiled again for about half an hour under stirring conditions. The solution turned orange in colour, indicating the formation of CdSe particles. In the rest of the paper, we denote these marcaptoacetic acid passivated CdSe particles as sample A.

2.4. Preparation of marcaptoacetic acid stabilized CdSe–CdS core–shell nanocrystals: sample B

For the preparation of coated CdSe–CdS particles, the above CdSe solution was cooled to 50 °C and 20 μl of $Cd(ClO_4)_2$ (0.1 M) and 20 μl of Na_2S (0.1 M) were added dropwise

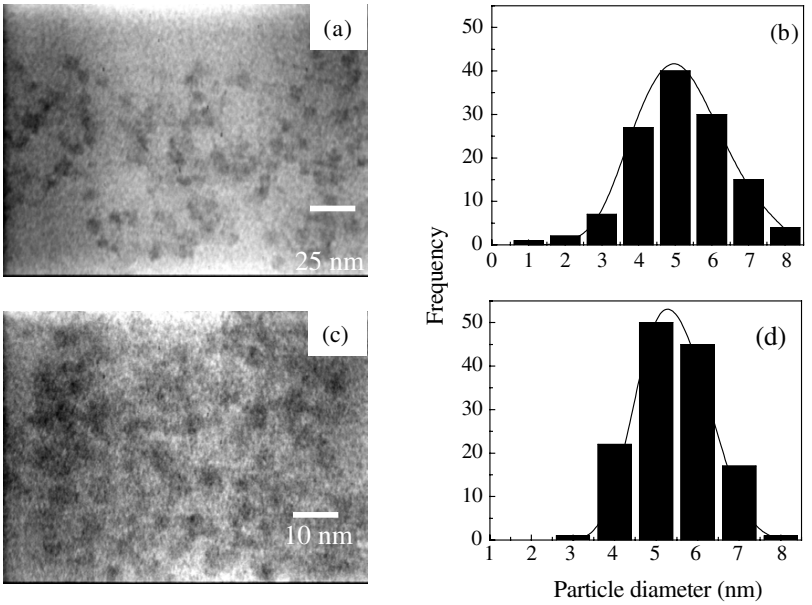

Figure 1. Low-magnification micrographs and histogram of the nanocrystals. (a) is the TEM micrograph and (b) is the corresponding histogram for sample A. Similarly, (c) is the micrograph and (d) is the corresponding histogram for sample B.

alternately under stirring conditions in N_2 atmosphere. After 30 min of stirring the solution turned orange-red in colour due to the formation of CdSe–CdS core–shell particles. In the rest of the paper, we denote these CdSe–CdS core–shell particles as sample B.

3. Average particle size and size distribution: TEM/HRTEM

Samples for TEM were deposited onto 300 mesh copper TEM grids coated with 50 nm carbon films. Samples A and B were suspended in water, and thus directly added dropwise onto the grid. The excess water was allowed to evaporate in air. The grids were examined in a JEOL 2010 microscope with ultra-high resolution (UHR) using a LaB_6 filament operated at 200 kV. TEM/HRTEM images of many nanocrystals for each sample were measured and analysed.

TEM was used to determine the particle size and size distribution of the aforementioned nanocrystals. Also, using high-resolution TEM, it is possible to confirm the core–shell structure of nanocrystals [3]. Low-magnification TEM micrographs are shown in figures 1(a) and (c) for samples A and B, respectively. Figures 1(b) and (d) are the histogram plots, obtained by measuring the sizes of many particles per sample. The size distributions for the nanoparticles are usually found to be log-normal:

$$P(d) = \frac{\bar{d}}{\sqrt{2\pi}\,\mathrm{d}\sigma} \exp\left(-\frac{\ln(d/\bar{d})}{\sqrt{2}\sigma}\right)^2. \tag{1}$$

Here $\bar{d}$ is the average size and σ is related to the size distribution of the particles (it is called the shape parameter of the distribution function). By fitting the frequency plot using equation (1) (solid lines in figure 1), we have estimated the average particle size ($\bar{d}$) and σ of the particles, which are listed in table 1. The size distribution of the particles is estimated to be more spread out for bare particles (sample A) compared to the other sample.

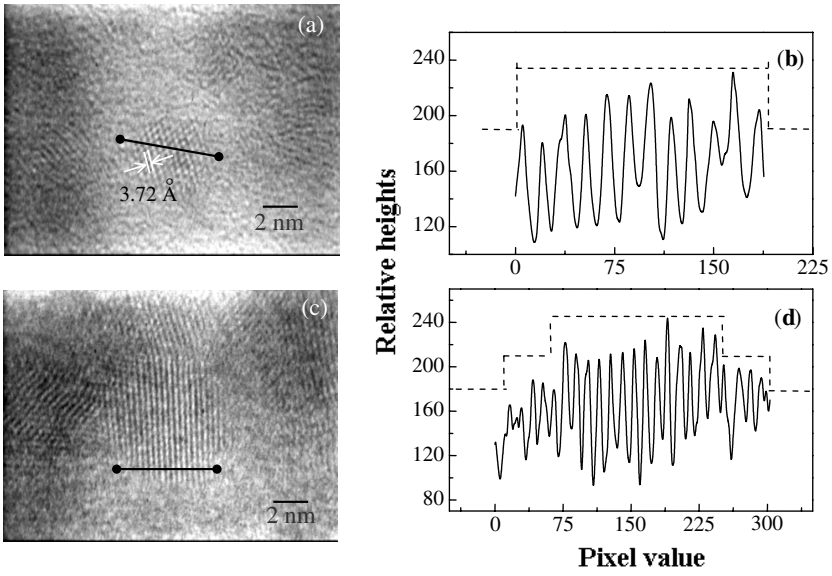

Figure 2. High-resolution TEM micrographs and corresponding line profiles for samples A and B.

Table 1. Comparison of the average size and size distribution of the particles in samples A and B as obtained from TEM images, and blue shift in optical absorption bands and confinement of phonons.

Sample	TEM		OAS		Raman
	$\bar{d}$ (nm)	σ	$\bar{d}$ (nm)	σ	$\bar{d}$ (nm)
Sample A	5.3 ± 0.4	0.25	6.0 ± 0.5	0.22	6.0 ± 1.0
Sample B	5.4 ± 0.4	0.15	7.0 ± 0.5	0.11	6.5 ± 1.0

HRTEM measurements provide convincing proof of the crystalline core–shell structure of the sample. Figures 2(a) and (c) show high-resolution micrographs of selected nanocrystals along the line profiles. The contrast in the image depends on the electron density in the object forming the image. Hence, CdS is expected to show less contrast than CdSe since the former has fewer electrons per unit cell. The line profile of the image contrast for samples A and B corresponding to the images are presented in figures 2(b) and (d). For sample A, we observe a smooth drop in the contrast near the edge of the nanocrystal. In comparison, the line profile of core–shell nanocrystals (sample B) exhibit a trend of a stepwise drop. The contrast can also be explained by the change in thickness of the nanocrystals, but it is not very probable that this would occur in such a steplike way. From the HRTEM images the average shell thickness of the particles in sample B has been estimated to be 1.2 nm.

From the micrograph (figure 2(a)), we have determined the lattice spacing in sample A to be 3.72 Å, which corresponds to the (100) plane of CdSe in the hexagonal phase [28].

4. Electron confinement: optical absorption spectroscopy

Figure 3(a) shows the optical absorption spectra for samples A and B. The absorption band energy (wavelength) from these samples is tabulated in table 2. The bulk bandgaps for CdSe

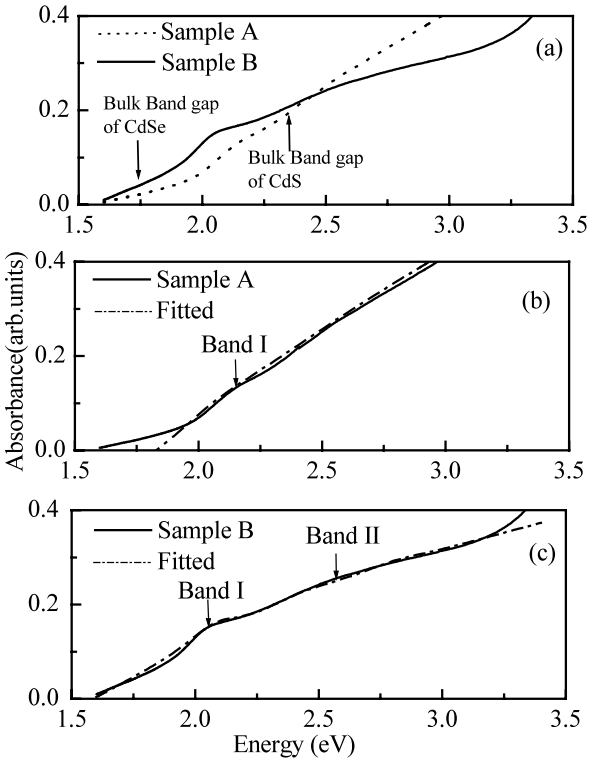

Figure 3. (a) Optical absorption spectra for samples A and B. The dotted line is the spectrum for CdSe particles and the solid line is for CdSe–CdS core–shell particles. The bulk bandgap positions for CdS and CdSe are shown by arrows. (b) and (c) The dashed dotted lines are the nonlinear least square fit to the experimental curves (solid lines) using an effective bond order model.

Table 2. Optical absorption bands for sample A and sample B.

Sample	Band I nm (eV)	Band II nm (eV)
Sample A	577 (2.15)	—
Sample B	606 (2.05)	477(2.60)

and CdS at room temperature are 1.74 and 2.42 eV, respectively. Sample A (bare CdSe particles) shows only band I at 2.15 eV in the optical absorption spectrum (see table 2). We have observed that due to CdS shell growth a new band (band II) at 2.60 eV appears in the optical absorption spectrum in addition to band I.

The blue shift in the optical absorption spectra of the particles from that for bulk CdSe and CdS arises from the confinement of charge carriers in the nanocrystals. Assuming the particles to be spherical, the optical absorption coefficient of the collection of the monodispersed particles of average diameter $\bar{d}$ at low temperature is given by

$$\alpha(E) = \sum \frac{f_i \Gamma_i}{(E - E_i)^2 + \Gamma_i^2}, \tag{2}$$

where f_i is the oscillator strength, E_i is the transition frequency and Γ_i is the half width at half maximum (HWHM) for the ith interband transition. Due to thermal broadening and inhomogeneous broadening due to the size distribution of the particles, equation (2) is

Table 3. The confinement energy (equation (4) with d in Å) for different electronic transitions.

Group		Electronic transition	Confinement energy (eV)	Type	f_i	A_i	x_i
Group I	CdSe	$1\Gamma_8^- - 1\Gamma_6^+$	0.42	1	4.85	55.50	1.23
		$1\Gamma_6^+ - 1\Gamma_7^-$	0.83	2	1.11	38.71	0.99
		$1\Gamma_6^+ - 1\Gamma_8^-$	0.84	2	0.10	38.71	0.99
		$2\Gamma_7^- - 1\Gamma_6^+$	0.72	3	0.61	70.35	1.17
		$2\Gamma_8^+ - 1\Gamma_8^-$	0.75	3	1.89	70.35	1.17
		$1\Gamma_7^+ - 1\Gamma_8^-$	0.78	3	0.62	70.35	1.17
		$3\Gamma_7^- - 1\Gamma_6^+$	0.76	3	0.01	70.35	1.17
Group II	CdS	$1\Gamma_8^- - 1\Gamma_6^+$	0.40	4	4.13	45.40	1.19
		$1\Gamma_7^- - 1\Gamma_6^+$	0.45	4	1.73	45.40	1.19

modified to

$$\alpha_{\text{observed}}(E) = B \sum_i \int_0^\infty d(d) \frac{P(d) f_i \Gamma_i}{[E - E_i(d)]^2 + \Gamma_i^2}, \tag{3}$$

where $P(d)$ is the log-normal size distribution of the particles, as in equation (1). The results of the single band effective mass approximation model do not agree with the optical absorption spectra of the nanocrystals because the model neglects intervalence band mixing and deviation from quadratic dispersion. This has been shown in the literature for bare CdSe or CdS particles and CdS–CdSe mixed crystals [18, 29]. We have assumed the results from the effective bond order model by Ramaniah and Nair on the interband transition in quantum dots of CdS and CdSe and considered the following transitions: $1\Gamma_8^- - 1\Gamma_6^+$, $1\Gamma_6^+ - 1\Gamma_7^-$, $1\Gamma_6^+ - 1\Gamma_8^-$, $2\Gamma_7^- - 1\Gamma_6^+$, $2\Gamma_8^+ - 1\Gamma_8^-$, $1\Gamma_7^+ - 1\Gamma_8^-$, $3\Gamma_7^- - 1\Gamma_6^+$, for the CdSe core $1\Gamma_8^- - 1\Gamma_6^+$, $\Gamma_7^- - 1\Gamma_6^+$ for the CdS shell [29]. Confinement energies for these transitions as obtained in [29] are tabulated in table 3. We have grouped these transitions in three types for CdSe and one type for CdS, according to their confinement energies. Since the oscillator strength is not very sensitive to the particle diameter $\bar{d} \geqslant$ 2–3 nm, the value of f_i corresponds to those of $d = 4.8$ nm for transitions in CdS and $d = 4.6$ nm for CdSe as obtained in [29]. The confinement energy (ΔE) for these four types of transitions versus particle size has been plotted in figure 4. For $\Delta(E)$ we have assumed the empirical relation [18]

$$\Delta(E) = A_i / d^{x_i}, \tag{4}$$

where A_i and x_i are constants for a particular transition. We have fitted the four types of transition with equation (4) (shown in figure 4) and estimated the values of A_i and x_i for these transitions, which are given in table 3. Taking $E_i(d) = E_g^{\text{bulk}} + A_i/d^{x_i}$ we have fitted the experimental optical absorption spectra, shown by dash–dotted lines in figures 4(b) and (c) for samples A and B, respectively. We have used only group I in table 3 for sample A, but both group I and group II in table 3 for sample B. It can be seen that the theoretical curves using the above EBOM model fit the experimental data for both sample A (band I due to interband transitions for CdSe) and sample B (band I due to interband transitions for CdSe and band II due to interband transitions for CdS) reasonably well. In this fitting procedure $\bar{d}$, σ and B are kept as fitting parameters. The slight discrepancies that exist may be related to a number of factors, like shape and surface structure uncertainties in the nanostructures. The values of average particle size and σ from the above analysis are tabulated in table 1. The same table also reveals the comparison between the average sizes of the particles obtained from Raman measurements (this will be discussed later) and HRTEM frequency plots.

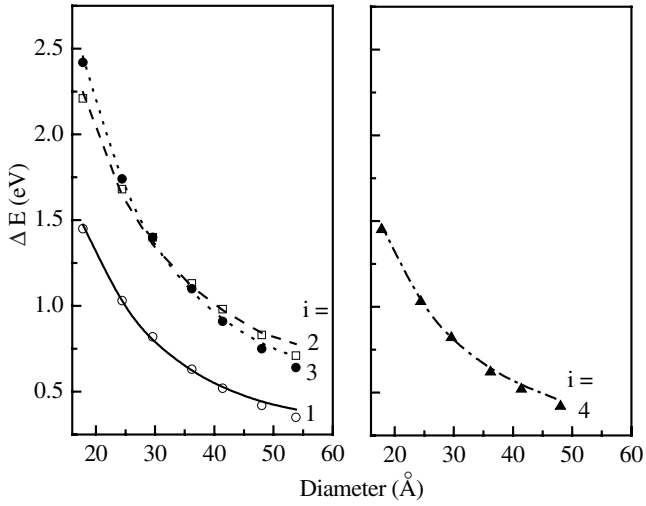

Figure 4. The variation in ΔE with respect to diameter, d, of the particle for different transitions in the effective bond order model for CdSe and CdS. The curve through the points is a fit to $\Delta E = A_i/d^{x_i}$.

5. Confinement of optic phonon and new surface phonons: Raman scattering

In order to understand the nature of phonon confinement and the appearance of new surface modes in our samples, we have performed Raman scattering studies. Raman spectra were obtained using a 1200 g mm^{-1} holographic grating, a holographic notch filter, and a Peltier cooled CCD detector. Spectra were taken using a 488 nm argon ion laser as an excitation source. The slit width of the spectrometer during the experiment was 50 μm. The first-order Raman spectra for the samples are shown in figure 5. Using the phonon confinement model of Campbell and Fauchet [12], the first-order Raman spectrum $I_c(\omega)$ is given by

$$I_c^j(\omega) = A^j \int_0^{q_{\max}^j} \frac{\mathrm{d}\mathbf{q}^j\, |C_j(0,\mathbf{q})|^2}{[\omega - \omega_j(\mathbf{q})]^2 + (\Gamma_{0j}/2)^2}, \tag{5}$$

where $\omega_j(\mathbf{q})$ and Γ_{0j} are the phonon dispersion curve and the natural line width (FWHM) of the corresponding bulk materials, and $C_j(0,\mathbf{q})$ is the Fourier coefficient of the phonon confinement function. A is an arbitrary constant. $j = 1$ for CdS and $j = 2$ for CdSe. For nanoparticles, it has been shown that the phonon confinement function which fits the experimental data best is $W(r,\bar{d}_z) = \exp(\frac{-8\pi^2 r^2}{\bar{d}_z^2})$, the square of the Fourier coefficient of which is given by $|C_2(0,\mathbf{q})|^2 \cong \exp(-\frac{q_z^2\bar{d}_z^2}{16\pi^2})$. Here, $\bar{d}_A$ is the average size of the spherical nanocrystals in sample A and $\bar{d}_B$ is the average diameter of the core in sample B. As the shell in a core–shell architecture is an epitaxial growth of a layer on the core, for the CdS shell component of particles in sample B we have used an additional phonon confinement function suitable for a two-dimensional layer, given by [12]

$$|C_1(0,\mathbf{q})|^2 \cong \exp\left(-\frac{q_1^2 t^2}{16\pi^2}\right)\left|1 - \mathrm{erf}\left(\frac{q_1 t}{\sqrt{32}\pi}\right)\right|^2 \tag{6}$$

where t is the average shell thickness for the particles. The average phonon dispersion in the bulk CdSe and CdS crystal for the LO phonon modes is taken as [30, 31]

$$\omega(q) = \omega_0^j - \Delta\omega^j(q_j^2) \tag{7}$$

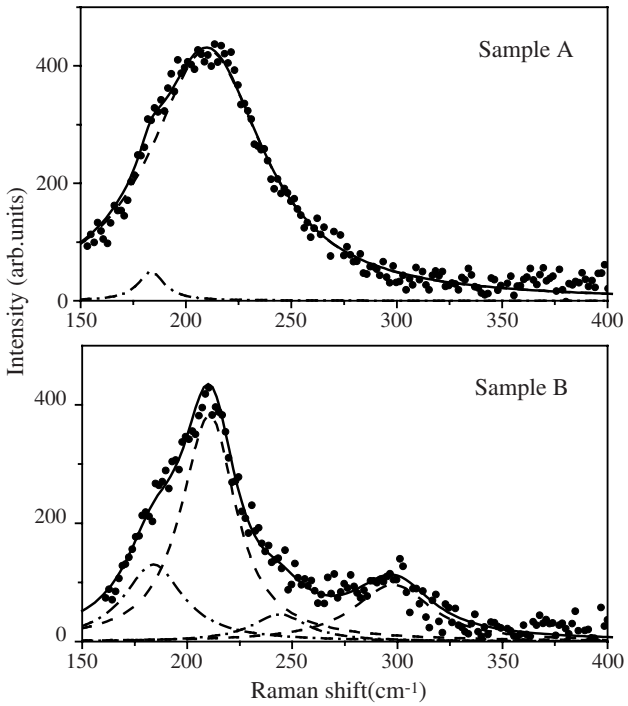

Figure 5. Raman spectra for samples A and B are shown by filled circles. Phonon confinement components and surface phonon components are given by dashed and dash–dotted lines, respectively. Solid lines correspond to the best fit to the experimental data using combined Raman line shapes.

which fits the experimental curve well in the direction of Γ–M up to $q_{\max} = 0.4.\omega_0^j$ is the corresponding bulk LO phonon frequency: $\omega_0^1 = 302\ \mathrm{cm}^{-1}$ and $\omega_0^2 = 213\ \mathrm{cm}^{-1}$. $\Delta\omega^j$ is the band width of the bulk LO phonon branch: $\Delta\omega^1 = 102\ \mathrm{cm}^{-1}$, $\Delta\omega^2 = 118\ \mathrm{cm}^{-1}$. In the above equations, q_j is taken in units of $2\pi/a_j$, where a_j is the lattice constant of the material. We have taken $a_1 = 5.82$ Å and $a_2 = 6.08$ Å [28].

We have also analysed the first-order optical phonons in core–shell structures and bare particles using the model proposed by Rodrigues *et al* [32]. In this model, the nanometre-sized crystallites are assumed to have the same atomic arrangement as that of bulk material. Modifying Loudon's derivation [33] of the Raman cross-section for infinite crystals, the cross-section for quantum dot structures has been estimated. For our samples, with size distribution, the simulated Raman line shape and estimated sizes of the particles obtained using Rodrigues model are the same as those found using the Campbell–Fauchet model. The finer features of the Rodrigues model get washed out when one includes the size distribution of the particles in the analysis, a fact which has been discussed in the literature [32].

In addition to the LO phonon peak, we have also observed additional peaks in the spectra for samples A and B. Keeping in mind the possibility of the presence of the surface phonons (SP) modes between longitudinal and transverse optical phonon modes, together with the confined optical phonon, we have fitted this additional peak with the Lorentzian function

$$I_{\mathrm{SP}}^j(\omega) = \frac{B\Gamma_{\mathrm{SP}}}{(\omega - \omega_{\mathrm{SP}})^2 + \Gamma_{\mathrm{SP}}^2}, \tag{8}$$

where ω_{SP} and Γ_{SP} are the peak position and the HWHM, respectively, for the SP mode. We fit the full spectrum for samples A and B by a combined line shape $I(\omega) = I_c^j(\omega) + I_{SP}^j(\omega)$. The best fits obtained for both samples are shown by the solid lines in figure 5. The phonon confinement components are shown by dashed lines and the surface phonon components are shown by dash–dotted lines in figure 5. In the fitting procedure, we have kept $\bar{d}_z$, t, ω_{SP}, Γ_{SP}, A and B as fitting parameters. For the best fit of the spectra the values of $\Gamma_{02}/2$ for sample A and sample B are taken to be 32 and 14.5 cm^{-1}. We attribute the variation in the value of $\Gamma_{02}/2$ from sample to sample to the difference in size distribution of the particles. From the nonlinear least square fit, the average particle size ($\bar{d}_A$) for sample A is obtained as 6.0 nm. The core diameter ($\bar{d}_B$)and shell (film) thickness, t, for sample B are obtained as 5.5 and 1.25 nm. This estimates the average particle diameter ($\bar{d}_B + t$) in sample B to be 6.75 nm. The diameters of the particles in sample A and B thus measured are very close to those estimated from optical absorption and TEM measurements (see table 1). We have observed SP modes for sample A at 183 cm^{-1} and CdSe-like and CdS-like modes in sample B at 180 and 244 cm^{-1}, respectively. The ratio of A/B is 2×10^3 for sample A, whereas the ratio of the same for CdS-like and CdSe-like modes in sample B is 85 and 68, respectively. It is to be noted that the analysis of the experimental results using the model proposed by Rodrigues *et al* leads to an identical result, when we include the size distribution of the core–shell particles.

Surface phonons in a core–shell structure in a host medium have been studied by the dielectric continuum approach [34], in which one takes into account the polar optical vibrations of each component in the core–shell–medium structure. In this model, the surface phonon dispersion relation is given by

$$\frac{\epsilon_2(\omega)}{\epsilon_m} = -\frac{[\gamma^{2l+1} - 1]\epsilon_1(\omega) + [1 + \gamma^{2l+1}(l+1)/l]\epsilon_2(\omega)}{[\gamma^{2l+1} - 1]\epsilon_2(\omega) + [1 + \gamma^{2l+1} l/(l+1)]\epsilon_1(\omega)} \tag{9}$$

where $\epsilon_1(\omega)$ and $\epsilon_2(\omega)$ are given by

$$\epsilon^j(\omega) = \epsilon_\infty^j \left[1 + \frac{\omega_{LOj}^2 - \omega_{TOj}^2}{\omega_{TOj}^2 - \omega^2}\right] \tag{10}$$

and ϵ_∞ is the high-frequency dielectric constant of the crystal. γ is the ratio of the diameter of the shell to that of the core for $l = 1, 2, 3 \ldots$. Here, we have $\gamma = \bar{d}/(\bar{d} - 2t)$, where t is the CdS shell thickness, as taken earlier. ω_{LOj} and ω_{TOj} are longitudinal and transverse mode phonon frequencies for CdS and CdSe. ϵ_m is the dielectric constant of the medium, marcaptoacetic acid in our case. Substituting equation (10) in equation (9) for both CdS-like and CdSe-like modes we obtain surface phonon branches for both the CdS shell and CdSe core materials in sample B. As before, we have taken the values of ω_{LO1} and ω_{LO2} as 302 and 213 cm^{-1} and the values of ω_{TO1} and ω_{TO2} as 238 and 168 cm^{-1}, respectively. The values of the other parameters are $\epsilon_m = 14.3$, $\epsilon_\infty^1 = 5.5$ and $\epsilon_\infty^2 = 8.9$ [35]. The average value of t is known from HRTEM and Raman measurements to be 1.2 nm.

We have observed that the SP mode for sample A is at 183 cm^{-1}, which is very close to the value of ω_{SP}(182 cm^{-1}) for pure CdSe particles, obtained from equation (10). On the other hand, the observed CdS-like SP frequency (244 cm^{-1}) from the shell component of the sample B is away from the frequency (252 cm^{-1}) of the same for pure CdS particles, estimated directly from equation (10). However, it is close to the value, 245 cm^{-1}, obtained from the combined equations (9) and (10) using the dielectric continuum model. The corresponding CdSe-like mode in sample B is expected to appear at 180 cm^{-1}, the same as observed in our experiment. The SP frequencies for the CdS-like and CdSe-like modes in sample A and B as obtained from the experiments and the above calculations are tabulated in table 4. The observed values of CdS-like and CdSe-like SP frequencies in sample B correspond to $l = 1$ in equation (9).

Table 4. Calculated and experimental CdS-like and CdSe-like SP frequencies in sample A and B. The frequencies are in units of cm^{-1}.

Sample	ω_{SP}CdSe(calc)	ω_{SP}CdSe(expt)	ω_{SP}CdS(calc)	ω_{SP}CdS(expt)
Sample A	182	183	—	—
Sample B	180	180	245	244

It is interesting to note that if CdSe–CdS were to form a mixed crystal in the solution, we expect (from the detailed theory of SP modes in mixed crystals) CdSe-like and CdS-like SP modes for sample B to appear at 204 and 267 cm^{-1}, respectively [18]. This is far away from what we have obtained experimentally. Thus, the above discussion implies that from the SP frequencies of the expected shell material, one can confirm the formation of core–shell-like particles, rather than the formation of mixed nanocrystallites or individual particles of shell material in the sample.

6. Conclusion

Our goal in this paper was to show electron and phonon confinement in the CdSe–CdS core–shell nanostructure. To this end, we have first confirmed the existence of the core–shell structure in our samples, prepared by a soft chemical route, using HRTEM images. Subsequently, to analyse the electronic transitions we focused on optical absorption measurements, supported by theoretical considerations of the effective bond order model. Furthermore, the first-order Raman line shape of the CdSe–CdS nanocrystals is quantitatively explained by taking into account both confined phonon modes and SP modes. We also demonstrated that due to passivated surface states CdS capped samples exhibit clear SP modes separated from the LO modes in core–shell type nanocrystallites. The frequencies of the SP modes are shown to match well with their calculated values as obtained from the dielectric continuum model. In summary, we have presented a technique to confirm the core–shell structure in this type of semiconductor nanostructure.

Acknowledgments

AR thanks DST and BRNS in India, for financial support.

References

[1] Schmid G (ed) 2004 *Nanoparticles: From Theory and Application* (Weinheim: Wiley–VCH GmbH & Co KGaA) and the references therein
[2] Spanhel L, Haase M, Weller H and Henglein A 1987 *J. Am. Chem. Soc.* **109** 5649
[3] Peng X, Schlamp M C, Kadavanich A V and Alivisatos A P 1997 *J. Am. Chem. Soc.* **119** 7019
[4] Wilson W L, Szajowski P J and Brus L E 1993 *Science* **262** 1242
[5] Kortan A R, Hull R, Opila R L, Bawendi M G, Steigerwald M L, Carroll P J and Brus L E 1990 *J. Am. Chem. Soc.* **112** 1327
[6] Hoener C F, Allan K A, Bard A J, Campion A, Fox M A, Mallouk T E, Webber S E and White J M 1992 *J. Phys. Chem.* **96** 3812
[7] Mews A, Eychmuller A, Giersig M, Schooss D and Weller H J 1994 *Phys. Chem.* **98** 934
[8] Danek M, Jensen K F, Murray B C and Bawendi G M 1996 *Chem. Mater.* **8** 173
[9] Hines M A and Sionnest P G 1996 *J. Phys. Chem.* **100** 468
[10] Pradhan N, Katz B and Efrima S 2003 *J. Phys. Chem.* B **107** 13843
[11] Danek M, Jensen K F, Murray C B and Bawendi M G 1994 *Appl. Phys. Lett.* **65** 2795

[12] Campbell I H and Fauchet P M 1986 *Solid State Commun.* **58** 739
[13] Richter H, Wang Z P and Ley L 1981 *Solid State Commun.* **39** 625
[14] Nemanich R J, Solin S A and Martin R M 1981 *Phys. Rev.* B **23** 6348
[15] Tsu R, Shen H and Dutta M 1992 *Appl. Phys. Lett.* **16** 112
[16] Sood A K, Jayaram K and Muthu D V S 1992 *J. Appl. Phys.* **72** 4963
[17] Roy A, Jayaram K and Sood A K 1994 *Solid State Commun.* **89** 229
[18] Roy A and Sood A K 1996 *Phys. Rev.* B **53** 12127
[19] Fuchs R and Kliewer K L 1968 *J. Opt. Soc. Am.* **58** 319
[20] Baranov A V, Rakovich Yu P, Donegan J F, Perova T S, Moore R A, Talapin D V, Rogach A L, Masumoto Y and Nabiev I 2003 *Phys. Rev.* B **68** 165306
[21] Norris D J, Scara A, Murray C B and Bawendi M G 1994 *Phys. Rev. Lett.* **72** 2612
[22] Xu L, Chen K, El-Khair H M, Li M and Huang X 2001 *Appl. Surf. Sci.* **172** 84
[23] Hoheisel W, Colvin V L, Johnson C S and Alivisatos A P 1994 *J. Chem. Phys.* **101** 8455
[24] Li J J, Wang A, Guo W, Keay J C, Mishima T D, Johnson M D and Peng X 2003 *J. Am. Chem. Soc.* **125** 12567
[25] Poznyak S K, Talapin D V, Chevchenko E V and Weller H 2004 *Nano Lett.* **4** 693
[26] Nanda J, Kuruvilla B A and Sarma D D 1999 *Phys. Rev.* B **59** 7473
[27] Liu S-M, Guo H, Zhang Z-H, Li R, Chen W and Wang Z-G 2000 *Physica* E **8** 174
[28] *X-ray Powder Diffraction, JCPDS file*
[29] Ramaniah L M and Nair S V 1993 *Phys. Rev.* B **47** 7132
[30] Trallero-Giner C, Debernardi A, Cardona M, Menendez Proupin E and Ekimov A I 1998 *Phys. Rev.* B **57** 4664
[31] Bliz H and Kress W 1979 *Phonon Dispersion Relations in Insulators* (Berlin: Springer) p 97 also see reference [2] p 63 & p 143
[32] Rodrigues P A M, Cardeira H A and Cardeira F 1989 *Int. J. Mod. Phys.* B **3** 1167
[33] Loudon R 1964 *Adv. Phys.* **13** 423
[34] Comas F and Trallero-Giner C 2003 *Phys. Rev.* B **67** 115301
[35] Lide D R (ed) *Handbook of Chemistry and Physics* (Boca Raton, FL: CRC Press)